International Journal for
Restoration of Buildings
and Monuments
Vol. 9, No 5, 513–534 (2003)

Hygral Behavior of Engineered Cementitious Composites (ECC)

M. B. Weimann and V. C. Li
Advanced Civil Engineering Materials Research Laboratory
Department of Civil and Environmental Engineering
The University of Michigan, Ann Arbor, MI, U.S.A.

Abstract

In this paper, the sorption isotherm and the hygral deformation of a tensile strain-hardening fiber reinforced engineered cementitious composite (ECC) is described using a physical model. The influence of using a low alkali content Portland cement on the physical mechanisms of drying shrinkage is discussed. From a durability point of view the crack width of a material as a result of restrained drying shrinkage deformations is more important than the total amount of drying shrinkage. In terms of crack width control the ECC shows a clear advantage compared to concrete. Due to the ultra-high strain capacity of ECC compared to concrete the use of ECC should be successful for applications where a high strain capacity and high durability are desirable.

Keywords: crack width, ECC, hygral deformation, sorption isotherm

Vergleich der hygrischen Eigenschaften von ECC mit Beton

Kurzfassung

In diesem Artikel werden die Sorptionsisotherme und die hygrischen Verformungen von einem unter direkter Zugbeanspruchung dehnungsverfestigenden „Engineered Cementitious Composite“ (ECC) mit einem physikalischen Modell beschrieben. Der Einfluss eines Portland-Zementes mit niedrigem Alkali-Gehalt auf das Trocknungsschwinden wird diskutiert. Für die Dauerhaftigkeit eines Werkstoffes ist die Rissweite, die bei einer Behinderung der Schwindverformung entsteht, wichtiger als der maximale Wert der hygrischen Schwindverformung. Die Rissweiten des ECC sind erheblich geringer als bei einem Beton. Aufgrund der ultra-hohen Bruchdehnung eines ECC im Vergleich mit einem gewöhnlichen Beton ist die Anwendung dieses Werkstoffes gerechtfertigt, wenn eine hohe Bruchdehnung und Dauerhaftigkeit verlangt werden.

Stichwörter: *Rissweite, ECC, hygrische Verformungen, Sorptionsisotherme*

1 Introduction

Moisture exchange of cementitious composites with the environment is from a durability point of view an important issue. In order to improve the durability of cementitious composites, the governing factors for diffusion controlled moisture exchange as well as for moisture dependent deformations should be understood.

Engineered cementitious composite (ECC) is a newly developed high performance fiber reinforced cementitious composite. ECC has tensile strain capacity of 3-5 %, several hundred times that of concrete or normal fiber reinforced concrete. While the ductility of ECC has been widely documented [1], its hygral behavior is much less reported. The focus of this research is on developing an understanding of the moisture induced macroscopic deformations of ECC based on the micro-mechanisms of hygral deformation of hardened cement paste.

It is widely known that the permeability of a cracked cementitious material is highly sensitive to the magnitude of crack width. Restrained drying shrinkage deformation of a cementitious composite leads to an eigenstress. Eigenstresses higher than the tensile strength of the material cause cracks. Through the cracks harmful fluids can penetrate into a composite and damage it. For the ECC investigated here the crack width due to restrained shrinkage is very small, in the order of 50 μm. It will be shown that this crack width can be further reduced by the use of a low alkali content Portland cement.

The objectives of this research are

1) determine experimentally the sorption isotherms and the hygral deformations of ECC
2) correlate these measured sorption isotherms and hygral deformations with physical models and
3) establish that crack width of ECC induced by restrained drying shrinkage is a material property.

The first and second section of the article briefly present pertinent theoretical models of moisture exchange, sorption isotherm and hygral deformation used to interpret experimental data described in a later section. Experimental methods and data of the diffusion coefficient, the sorption isotherm, the hygral deformation as well as the crack width for ECC will be presented in the following sections. Thereafter follows a discussion of the results and conclusions.

2 Mechanism of Moisture Exchange and Description of the Sorption Isotherm

Capillary porous cement paste as a part of cementitious composites contains moisture either in the form of capillary condensed water or as adsorbed water on the inner surfaces of pores. Due to the fact that a cementitious material is water satura-

ted after production the composite starts drying when it is exposed to a relative humidity lower than 100 %. The drying process leads to a moisture loss in the pores due to a concentration gradient of moisture with the environment. The time dependent moisture loss for a cementitious composite which is not in hygral equilibrium with the environment can be described with Fick's second law of diffusion [2]:

$$\frac{du(RH(x,y,z),t)}{dt} = -div(D(u)\cdot grad(u)) \tag{1}$$

Here D is the moisture dependent diffusion coefficient and u is the moisture content which is a function of RH (x, y, z) and time t. RH is a function of the location (x, y, z). A known diffusion coefficient allows a calculation of a time dependent moisture distribution of a structure. The value D will be calculated from the experimentally determined data of the moisture loss as a function of time and RH for ECC.

The Kelvin equation describes the maximum radius of pores, which are water saturated as a function of the relative humidity [3]. Due to the effect of capillary condensation pores in a cementitious composite are water saturated even when the water vapor partial pressure is lower than the saturated water vapor partial pressure. Figure 1 illustrates the largest radius of pores, which are filled due to capillary condensation as a function of the relative humidity. At 40 % RH all pores are empty according to the Kelvin equation due to the fact that no pores with a radius smaller than 1nm exist [4] in a cementitious material. For RHs lower than 40 % the surfaces of the colloidal CSH-gel particles are covered with adsorbed water molecules.

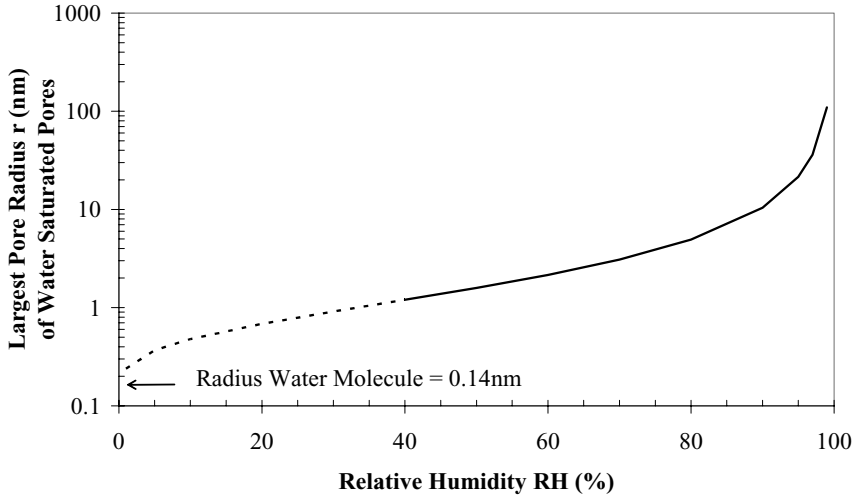

Figure 1: Graphical illustration of the Kelvin equation

Eq. 2 describes the sorption isotherm of a cementitious composite between 0 % and 100 % RH for a composite in hygral equilibrium with the environment [5]. Here $RH = 100 \cdot P/P_s$ where P_s= saturated water vapor partial pressure and P = water vapor partial pressure.

$$u(RH) = \frac{u_m \cdot q \cdot P_x}{(P_s - P_x) \cdot (1 + (q-1) \cdot (P_x / P_s))} + a \cdot \exp((b \cdot (P - P_c)) \qquad (2)$$

where

u = moisture content [Vol.-%]

u_m = moisture content of a monolayer [Vol.-%]

q = interaction parameter [-]

P = water vapor partial pressure [Pa]

a = empirical parameter [Vol.-%] (a = 0, for all $P \leq 952 Pa$)

b = empirical parameter [1/Pa]

P_x = P, for all $P \leq 952 Pa$, otherwise P_x = 0 Pa

P_c = 952 Pa

P_s = 2380 Pa

Between 0 % and 40 % RH we can describe the sorption of water molecules on the surfaces of CSH-gel particles with the BET-equation [6] (first term of Eq. 2). According to BET the covering of pore surfaces with increasing RH starts first with a monolayer of water molecules and than successive with the next layer of water molecules until 40 % RH. At RH higher than 40 % capillary condensation starts filling the pores, which can be described with Kelvin's equation. The second term of Eq. 2 describes the moisture uptake due to capillary condensation.

Equation 2 describes the moisture content in a cementitious element in hygral equilibrium with the environment. Drying of a structural element leads to a hygral disequilibrium. In order to calculate the time and spatial dependent moisture distribution in a structural element subject to drying, Eq. 1 must be used. The moisture loss in a cementitious element causes a moisture dependent deformation. The mechanism of the moisture dependent deformations is the subject of the following section.

3 Mechanisms of Moisture Dependent Deformations

Moisture dependent deformations like drying shrinkage in a cementitious material can be attributed to changes at the micro-level in a) surface energy of CSH-gel particles b) disjoining pressure between surfaces of CSH-gel particles, and c) capillary under-pressure [7]. The disjoining pressure defines the force of interaction per unit area of bodies that are separated by a thin parallel interlayer [8], and is a superposition of three forces. These forces are a) an attractive van der Waals force b) a repulsive electrostatic force and c) a repulsive steric force. The steric force may be altered by the introduction of polymers. This will not be the focus in this paper. The electrostatic force is influenced by the charge composition of the pore solution of the cementitious composite. The importance of the deformation micro-mechanisms varies with the relative humidity [7].

In the following we focus on hygral deformation instead of drying shrinkage in order to be able to explain the influence of different pore solutions on the micro mechanisms of deformations at changing RH. The hygral deformation at a given RH can be computed from the difference between the steady state drying shrinkage value of the dry state and the steady state drying shrinkage value at that RH. The total hygral deformation of ECC is described by using the Munich model, which was originally developed for cement paste [9, 10]. It was shown that the Munich model also works for concrete and brick [5]. According to this model, which assumes that the capillary forces are approximately independent of RH [7, 11], the total amount of the hygral deformation results from one part, which is due to a change of the surface energy of CSH-gel particles and from a second part, which is the result of a disjoining pressure between CSH-gel surfaces:

$$\varepsilon_{hyg,total}\left(RH\right) = \varepsilon_{hyg,surface}\left(RH\right) + \varepsilon_{hyg,disjoining\ -\ pressure}\left(RH > 40\right) \tag{3}$$

The first term of Eq. 3 can be related to surface energy change according to the Bangham equation [12]:

$$\varepsilon_{hyg,surface}\left(RH\right) = \lambda \cdot \Delta\gamma\left(RH\right) \tag{4}$$

Here λ is a function of the stiffness of the porous material [13]. The change of specific surface energy Δγ can be calculated from the experimentally measured adsorbed water u at different RH [14,15,16]:

$$\Delta\gamma(RH) = -\frac{R \cdot T}{M \cdot A}\int_0^P \frac{u}{P}dP \tag{5}$$

Here R = universal gas constant, T = absolute temperature, M = mol volume of water, A = specific surface area and P= water vapor partial pressure, which depends on RH and u=adsorbed water volume. For the second term of Eq. 3 we can write [5]

$$\varepsilon_{hyg,\ disjoining-pressure}\left(RH_x\right) = c\cdot\left(RH_x - RH_{40}\right)^2 + d\cdot\left(RH_x - RH_{40}\right) \qquad (6)$$

Here c and d are empirical parameters. Equation 6 is valid for $RH_x \geq \mathrm{RH}_{40}$ with $RH_{40} = 40\%$.

The influence of the pore solution of a cementitious composite on the disjoining pressure was discussed in the literature [7]. The authors have compared the influence of a low alkali content (0.6 M.-%) Portland cement and a normal alkali content (0.9 M.-%) on the drying shrinkage deformation of ECC [17]. A reduction of the alkali content causes a lower disjoining pressure. This can be explained with the DLVO-theory [7, 18]. A lower disjoining pressure leads to a smaller equilibrium distance between CSH - gel particles at 100 % RH. A smaller equilibrium distance between the particles at 100 % RH leads to a lower macroscopic deformation of cementitious materials when drying occurs [17].

4 Differential Drying Deformation and Durability

This section highlights the linkage between durability, micro-cracking, hygral deformation (Eq. 3), and moisture distribution (Eq. 1 and 2).

Drying of a cementitious element leads to a moisture loss in the material. As mentioned earlier it is possible to calculate the time dependent nonlinear moisture distribution of a material with a known diffusion coefficient and initial moisture content. Figure 2 shows calculated nonlinear moisture distributions u (x, t) with Eq. 1 at seven different drying times [19]. The concrete structural element has a thickness of x and dries symmetrically about the mid-section. At the beginning of drying (t = 0) the element is in hygral equilibrium with 100 % RH and than exposed to an environment with 50 % RH. The moisture content at the beginning (t = 0) and at the end (t = ∞) of the drying process can be described with Eq. 2.

Due to the nonlinear moisture distribution the element suffers a differential drying deformation. If we assume the element hypothetically as a superposition of infinitesimally unbounded layers, each layer should deform independently in the case of free drying shrinkage. This is shown in Figure 3a. Figure 3b shows the differential drying shrinkage deformations for monolithically interconnected layers. The time dependent shrinkage deformation depends on the modulus of elasticity, the tensile strength, the strain-softening or strain-hardening behavior as well as the diffusion coefficient of the investigated material [20]. Eq. 3 describes the hygral deformation of the element in equilibrium with 50 % RH.

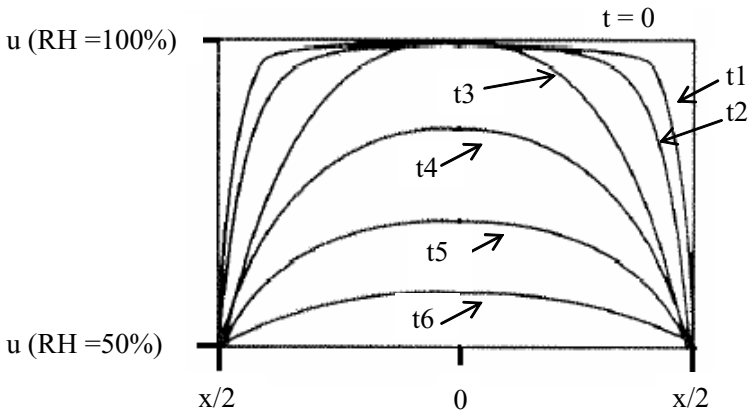

Figure 2: Time dependent nonlinear moisture distribution u (x, t) in a structural element, adapted from [19]

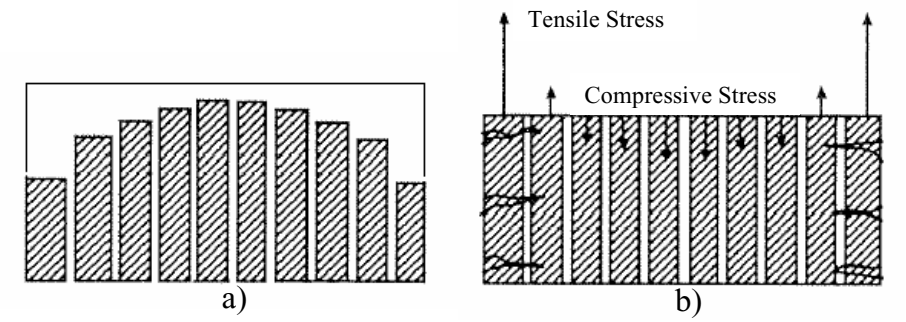

Figure 3: a) Free differential drying shrinkage deformations
b) Restrained differential drying shrinkage deformations and eigenstress, adapted from [19]

Due to the restraint of the layers the drying leads to the development of an eigen-stress in the element. The inner part of the element experiences compressive stress and the outer part tensile stress. The highest value of the tensile stress develops on the exposed surface layer because the moisture gradient has the highest value there. For tensile stresses higher than the tensile strength, micro-cracking starts at the exposed surface. Through these micro-cracks fluids like water or carbon dioxide can penetrate into the material. If the penetrating water contains water-soluble chlo-

rides and if a certain amount of chloride reaches the reinforcement of a cementitious element, corrosion can start. The corrosion products lead to a volume expansion, which can result in surface spalling of the concrete cover. Penetrating carbon dioxide leads to a reduction of the pH-value in a cementitious material. If the pH-value at the reinforcement drops below 9, corrosion of the reinforcement starts. The above mentioned reasons show clearly that a reduction or even better an avoidance of micro-cracks is desirable in terms of durability of a cementitious material.

5 Experiments

In this research project we will investigate an ECC with a normal alkali content (0.9 M.-%) Portland cement and an ECC with a low alkali content (0.6 M-%) Portland cement. These ECCs are reinforced with 2 % by volume of PVA (PolyVinyl Alcohol) fibers. An ECC-Matrix composition with normal alkali content Portland cement and without fibers will also be investigated. A small amount of **H**ydroxy-**P**ropyl-**M**ethyl**C**ellulose (HPMC) was added to the ECC-Matrix composition to prevent segregation. Normal concrete is included in these experiments for comparison. The mix compositions of the investigated materials are shown in Table 1.

Using an uniaxial direct tension test [21], the tensile stress-strain curves of ECC and concrete were determined. The objective of this test in combination with the free drying shrinkage test (described below) is to show, that the tensile strain capacity of ECC is higher than the drying shrinkage deformation. This means, that the crack width of ECC under restrained drying shrinkage is a material property. The drying shrinkage deformation of concrete is much higher than the tensile strain capacity of concrete, implying that the crack width depends on the specimen size and geometry in the case of concrete.

Table 1: Mix compositions of the investigated materials (SP = super plasticizer; m= maximum aggregate size)

	Aggregates [kg/m^3]	Cement [kg/m^3]	Water [kg/m^3]	Fly Ash [kg/m^3]	SP [kg/m^3]	Fiber [kg/m^3]
ECC (0.9 M.-%)	m < 150 μm 467	583	298	700	17.5	26
ECC (0.6 M.-%)	m < 150 μm 467	low alkali 583	298	700	17.5	26
ECC-Matrix	m < 150 μm 477	595	304	714	17.9 +HPMC	-
Concrete	m < 25 mm 1728	432	192	-	-	-

Free drying shrinkage measurements were made for all four materials as a function of drying time and RH. Drying shrinkage measurements, with a set-up as shown in Fig. 4a, were conducted based on ASTM C157/C157-99 and ASTM C596-01 [22] standards. These measurements clarify the differences in drying shrinkage behavior of the different mixes. In addition, the water mass loss per volume of the specimens was determined in order to calculate the volume content of moisture u, needed to calculate the change of the specific surface energy at different RH, the sorption isotherm and the diffusion coefficient. It should be noted that the sorption isotherm and the hygral deformation curves reported and discussed in this paper were obtained from a first cycle drying (100 % RH to 0 % RH) of the material. Strictly speaking, the rewetting from the dry state is expected to produce a different sorption isotherm and hygral deformation due to known hysteresis effect.

Fourteen specimens for each mix were cast and demoulded after one day. After two days of storage at RH = 100 % two specimens of each mix were stored in RH= 93 %, 85 %, 75 %, 66 %, 33 %, 12 % and 0 %, obtained by using saturated salt solutions in different desiccators [23, 24]. The drying shrinkage deformation and mass loss were measured as a function of drying time until hygral equilibrium was reached. The length change was measured with an accuracy of 1 μm. The mass loss was measured with an accuracy of 1mg. After all specimens had reached hygral equilibrium, the specimens stored at 0 % RH were dried in an oven at 105 °C until the mass is constant. After removing from the oven, the specimens were allowed to cool down to room temperature in order to measure the hygral length change due to moisture loss. When the specimens reached thermal equilibrium with room temperature, the length change and mass loss were determined and considered as values at RH = 0 %.

In order to investigate the number and width of drying shrinkage induced cracks, the restrained shrinkage ring test [25] was adopted (Fig. 4b). Two specimens of each mix were cast. During casting a thin plastic foil, covered cardboard paper cylinder was used as an outer mold which was removed three days after casting. Subsequently, the specimens were exposed to RH = 50 %. Drying of the specimen leads to an internal radial pressure in the specimen resulting from the restraint of the hygral deformation by the steel ring. From the dimensions of these specimens, it can be shown that the specimens were subject to an approximately uniaxial tensile stress state during restrained shrinkage. Figure 5 illustrates the measurement of the crack width, determined as an average value for each crack at three different locations as a function of the drying time.

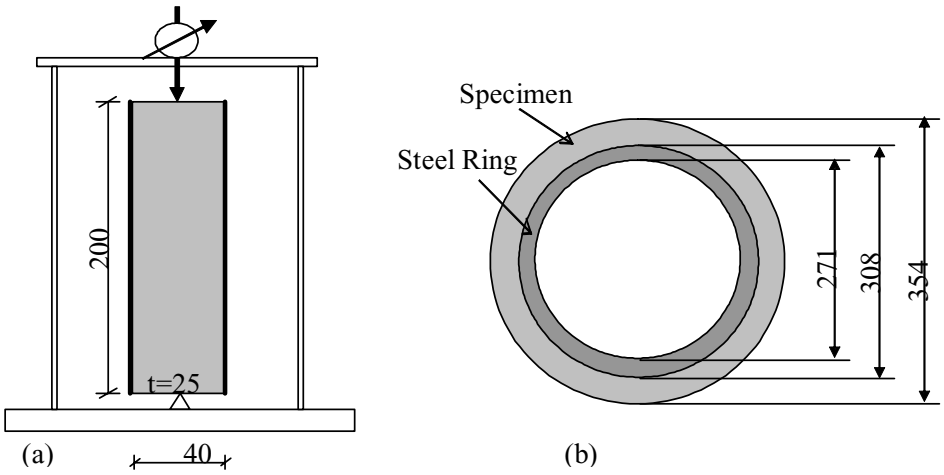

Figure 4: Experimental set- up:
(a) Free drying shrinkage test and
(b) Restrained shrinkage ring test (Dimensions in mm)

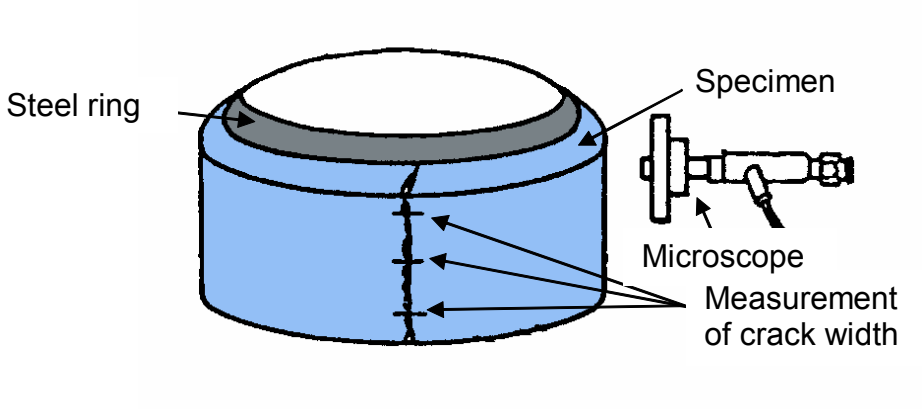

Figure 5: Ring test for determination of the crack width

6 Results and Discussion

The sorption isotherms of the investigated materials are shown in Figure 6. The dotted lines of Figure 6 are the calculated values of the moisture content according to the BET-Theory. The calculation of the moisture content according to the BET-theory requires the determination of the constants u_m and q in Eq. 2. Therefore we put the first term of Eq. 2 in the form [6]:

$$\frac{P_x}{u \cdot (P_s - P_x)} = \frac{1}{u_m \cdot q} + \frac{q-1}{u_m \cdot q} \cdot \frac{P_x}{P_s} \tag{7}$$

A plot of $P_x/u \cdot (P_s - P_x)$ against P_x/P_s gives a straight line and the constants u_m and q can be calculated from the intercept and slope. Their values for each material are given in Table 2. The solid line of Figure 6 corresponds to the moisture content in the pores due to capillary condensation and is described by the second term of Eq. 2. The parameters a and b are also shown in Table 2.

Table 2: Parametric values of u_m, q, a and b of the investigated materials

	u_m [Vol.-%]	q [-]	a [Vol.-%]	b [1/Pa]*10^{-3}
ECC (0.9 M.-%)	8.0	315	13.2	0.30
ECC (0.6 M.-%)	8.0	315	13.2	0.28
ECC-Matrix	8.5	391	14.2	0.30
Concrete	2.2	48	3.6	1.02

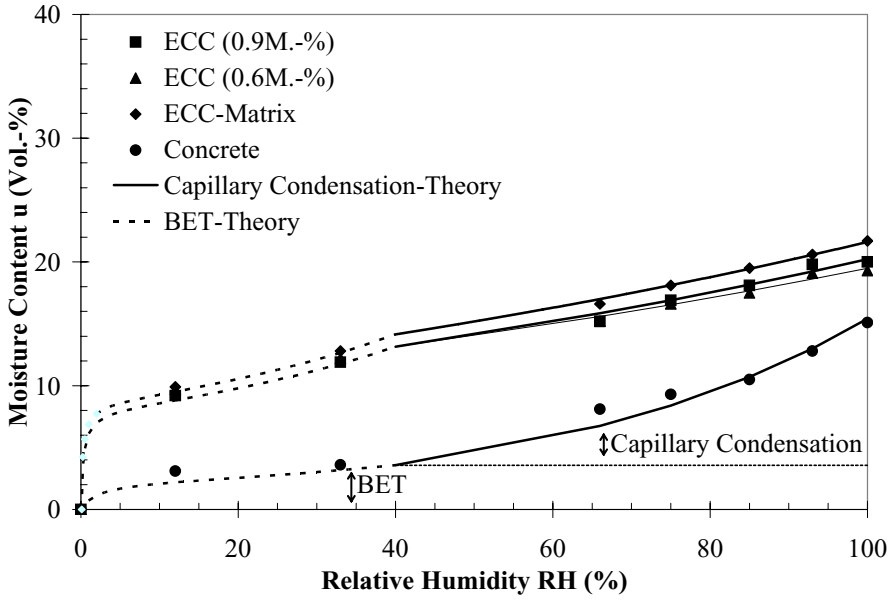

Figure 6: Sorption isotherm of the investigated materials

Figure 6 shows that the maximum moisture content and therefore the pore volume of the investigated ECCs is higher compared to the investigated concrete. This is likely due to the higher cement paste content of the ECCs. The higher parametric value u_m of ECC (Tab. 2) compared to concrete indicates that the amount of moisture, which is necessary to cover all pore surfaces with a monomolecular layer of water is higher for ECC. The lower value b (Tab. 2) of ECC compared to concrete suggests that the moisture content due to capillary condensation of ECC is lower. From the higher value of u_m and the lower value of b we can assume that the pore size distribution of ECC is different from the investigated concrete. The mean value of the pore size distribution of ECC is expected to shift to a smaller pore radius. The parameter a indicates the maximum moisture content of the materials, which can be described with the BET-theory. Details about the parameter q can be found in the literature [6].

The diffusion coefficient D of the investigated materials as a function of the relative humidity is shown in Fig. 7. The diffusion coefficients are calculated from the data of the moisture loss as a function of the drying time and RH using a "finite volume" program based on Eq. 1. The program compares the calculated data of the moisture loss with the experimental data in order to minimize the square of distance between the calculated and the experimental data. More details of the computational procedure can be found in the literature [5].

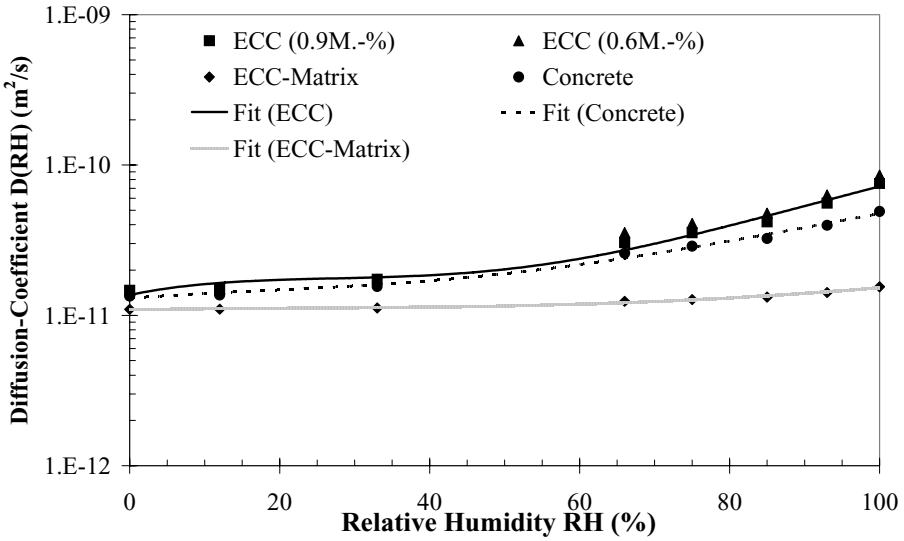

Figure 7: Diffusion coefficient of the investigated materials

We can see from Fig. 7 that the diffusion coefficients of concrete and ECC are similar for RHs lower than 65 %. The diffusion coefficients of all investigated materials show an increase with increasing RH. The higher diffusion coefficient of ECC compared to the investigated concrete is expected to lead to smaller moisture gradients in ECC. This causes a smaller eigenstress in ECC and should therefore improve the durability of ECC compared to concrete.

Figure 8 shows the calculated change of the specific surface energy as a function of the relative humidity based on Eq. 5 and using the moisture content per volume for the investigated materials measured at 0 %, 12 % and 33 % RH. The dotted lines in Fig. 8 are logarithmic fits to the change of specific surfaces energy for different RH in the form

$$\Delta\gamma = A \cdot \ln(RH) + B \tag{8}$$

From the experimental data $\Delta\gamma$, the values of A and B are determined for each material and reported in Table 3.

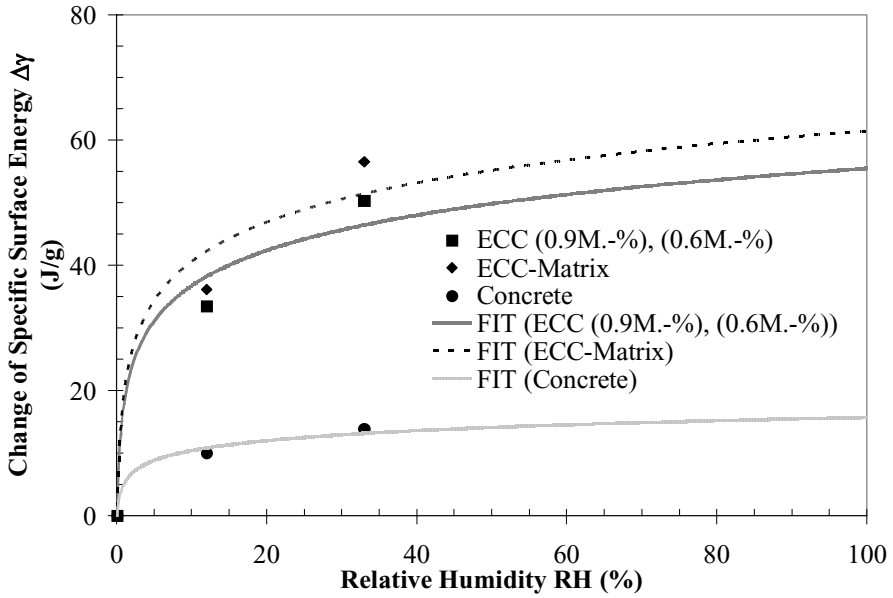

Figure 8: Experimental data and theoretical fits of change of specific surface energy as a function of the relative humidity for the investigated materials

Table 3: Parametric values of the investigated materials

	A **[J/g]**	B[**J/g]**	λ **[g/J] x10^{-3}**	**c [-] x 10^{-5}**	**d [-] x 10^{-4}**
ECC (0.9 M.-%)	8.2	17.9	2.3	2.0	+7.1
ECC (0.6 M.-%)	8.2	17.9	2.3	3.9	-2.8
ECC-Matrix	9.1	19.8	1.6	4.2	-1.1
Concrete	2.3	5.1	4.0	1.9	-3.0

In Figure 9 the hygral deformation of the investigated materials dried to different RHs is plotted as calculated from the drying shrinkage data as the difference between the steady state drying shrinkage value in the dry state (0 % RH) and the steady state drying shrinkage value at specific RHs. At 100 % RH ECC (0.6 M.-%) shows a lower hygral deformation due to the lower equilibrium distance between CSH-gel particles [17] produced with low alkali content (0.6 M.-%) Portland cement compared to normal alkali content (0.9 M.-%) Portland cement.

Using Eq. 3, the total hygral deformation of the investigated materials can be rewritten in the following form:

$$\varepsilon_{hyg,\,total} = \lambda \cdot (A \cdot \ln(RH) + B) + c \cdot \left(RH_x - RH_{40}\right)^2 + d \cdot \left(RH_x - RH_{40}\right) \qquad (9)$$

The first term is from Eq. 4 and 8 for $\varepsilon_{hyg,\,surface}$. The second and third terms are from Eq. 6 for $\varepsilon_{hyq,\,disjoining-pressure}$ [5]. Equation 9 is valid for $RH_x \geq RH_{40}$ with RH_{40} = 40 % . For $RH_x < RH_{40}$, only the first term in Eq. 9 applies. The parametric values λ, c and d for the investigated materials shown in Table 3 were obtained by fitting Eq. 9 to the total hygral deformation data reported in Fig. 10. The parametric values of λ are in the same order of magnitude as concrete reported in the literature [5].

Figure 10 shows the uniaxial tensile stress-strain curve and the crack width for ECC (0.9 M.-%). For comparison a typical stress-strain curve of a concrete taken from the literature is included [26]. Note that the post-peak deformation of the concrete is not a real strain, but reflects the crack opening within the gage length.

The strain values of the concrete have been expanded by a factor of 10 to show the curve more clearly. The crack width in the ECC was obtained by monitoring the opening of one of the many multiple cracks as the specimen strain increased. The crack width increases with strain up to about 1 % and then stabilizes at a steady state value of about 60 μm until fracture localization at ε = 5.2 %.

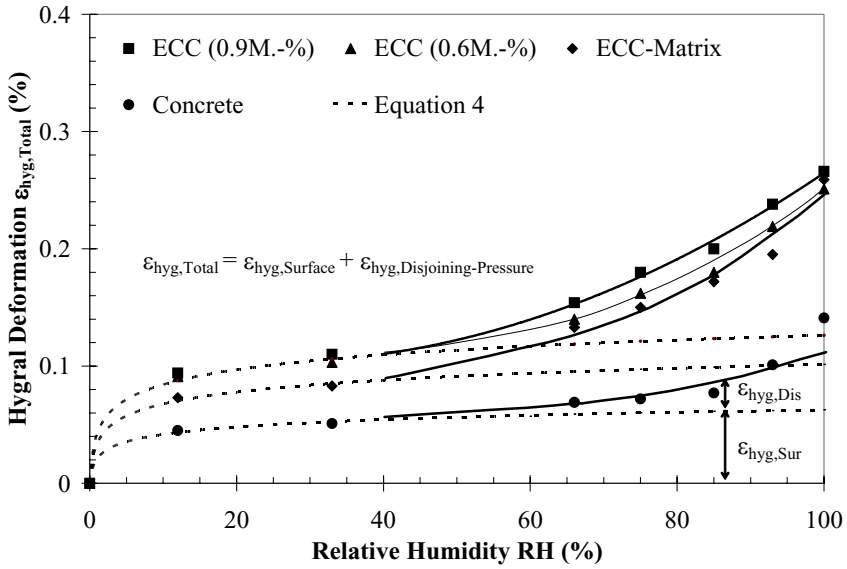

Figure 9: Experimental data and theoretical curves of hygral deformation as a function of the relative humidity for the investigated materials

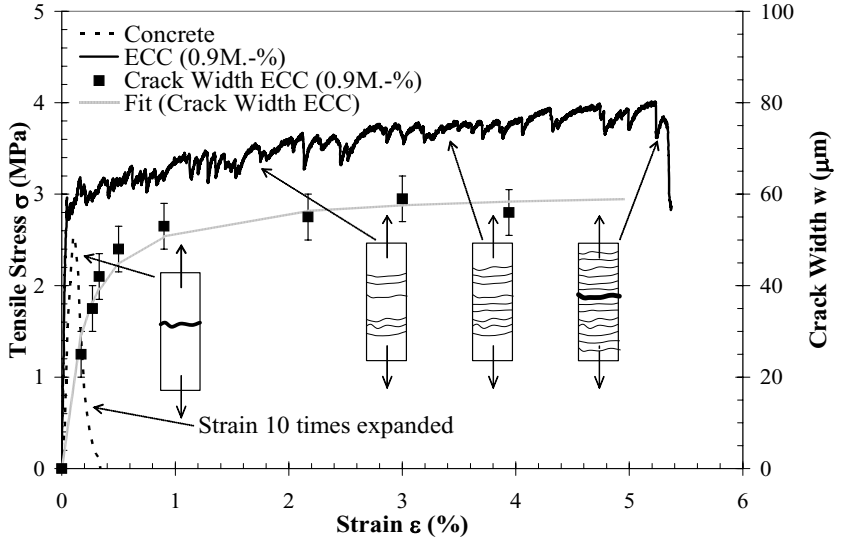

Figure 10: Tensile stress-strain curve of ECC (0.9 M.-%) and concrete. The crack width as a function of tensile strain is also shown for the ECC

The measured crack width w as a function of the drying time from the ring-test is shown in Fig. 11. The average crack width in the ECC is almost 20 times smaller compared to the crack width in concrete. A cracked concrete with a crack width smaller than 50 μm has been shown to have the same permeability as an uncracked material [27]. From a durability point of view the ECC can be considered an effectively uncracked material.

As can be observed in Fig. 9, the typical drying shrinkage deformations of ECC are lower than 0.3 %, so that even a small reduction of the tensile strain has a great influence of the crack width (Fig. 10). This is the reason why an ECC made with a low alkali content (0.6 M.-%) Portland cement shows a lower crack width compared to an ECC produced with a normal alkali content (0.9 M.-%) Portland cement. Figure 11 shows that the ECC (0.6 M.-%) has a crack width of 31 μm compared to 46 μm for ECC (0.9 M.-%).

The ECC-Matrix shows a crack width over 5 times higher than the concrete. Clearly, the fibers of the ECC leads to a 100-fold reduction in the crack width compared to the ECC-Matrix although the total hygral deformation (100 % to 0 %) of both is the same.

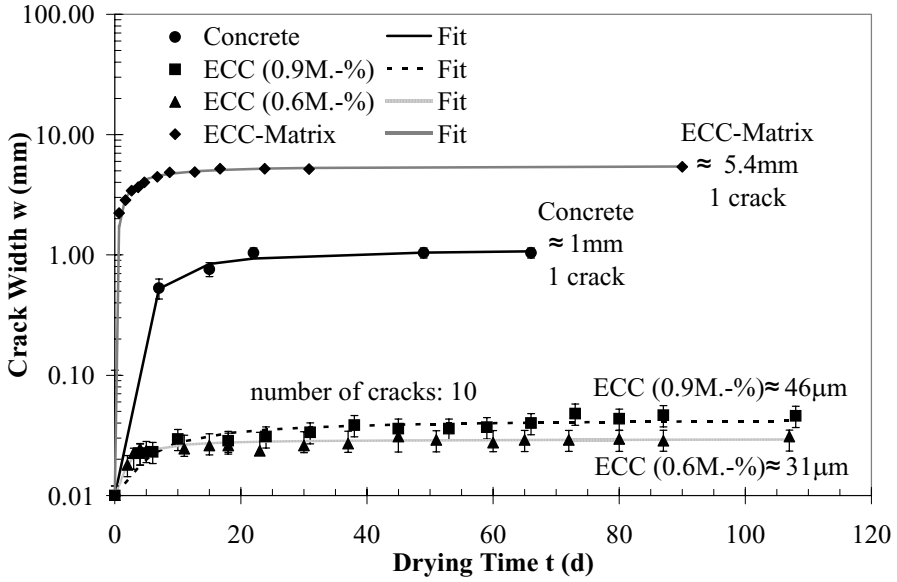

Figure 11: Crack width development as a function of drying time (at RH=50%)

The drying time when the first crack appears shows large differences. For the brittle ECC-Matrix the one and only crack appeared after 1 day drying time. The quasi-brittle concrete took seven days of drying before the crack appeared. The first crack for the ductile ECC appeared after four days of drying. These cracks are hardly visible to the naked eye. An optical microscope is necessary to measure the crack width.

7 Conclusions

The sorption isotherm of ECC from the dry state (0 % RH) to 40 % RH can be explained by sorption of water molecules onto the inner surfaces of the cementitious material. The filling of pores from 40 % RH to 100 % RH is due to capillary condensation. This is demonstrated by the good fit between theory and experimental data shown in Fig. 6. These results clarify that the moisture uptake of ECC, while higher than concrete, is governed by the same mechanisms as for concrete.

The hygral deformation of ECC can be explained by an expansion of CSH-gel particles due to a change of surface energy and by a repulsive disjoining pressure for RH > 40 %. A reduction of disjoining pressure leads to lower drying shrinkage. Methods to reduce the disjoining pressure include the use of a low alkali content (0.6 M.-%) Portland cement, the use of alkali free mixing water, and the addition of trivalent ions in the concrete composition, or any combination of the above.

ECC produced with a low alkali content (0.6 M.-%) Portland cement leads to a 5 % reduction in free drying shrinkage deformation (Fig. 9) and a 30 % lower crack width at 50 % RH compared to an ECC produced with a normal alkali content (0.9 M.-%) Portland cement (Fig. 11). It is desirable to produce ECC with low alkali content Portland cement in order to improve the durability for RH < 50 %. At RH > 50 %, the influence of alkali content on free drying shrinkage and crack width of the ECCs investigated is negligible.

The crack width of ECC under restrained drying shrinkage is about 30-50 μm (depending on cement type) at 50 % RH for the mix compositions tested (Fig. 11). This crack width is below the steady state crack width during strain-hardening (Fig. 10). In terms of durability the crack width is more important than the amount of free drying shrinkage, so that ECC should be more durable than concrete despite the higher free drying shrinkage. Since the free shrinkage (shown as hygral deformation in Fig. 9) is less than 0.3 %, and is much below the tensile strain capacity of 5 % (Fig. 10), the restrained shrinkage cracking phenomena is occurring in the strain-hardening stage. Hence the shrinkage crack width is a material property, implying that the shrinkage induced crack width of ECC is independent of structural dimension or reinforcement ratio.

The moisture dependent diffusion coefficients of the investigated ECC and concrete are similar up to 65% RH and show an increase as a function of RH. For RH higher than 65% the diffusion coefficient D of ECC is higher than the diffusion coefficient of the investigated concrete (Fig. 7). The higher diffusion coefficient of ECC compared to the investigated concrete is expected to lead to smaller moisture gradients in the materials. The smaller moisture gradient causes a lower eigenstress in the material, which is desirable in terms of durability.

The depth of penetration of water and aggressive agents due to capillary suction in a porous material is inversely proportional to the width of cracks or radius of pores, which are assumed as capillary tubes. Treatment of the surface of ECC with a hydrophobic agent may be useful to further minimize penetration of water and aggressive agents into an ECC cover and protect the steel reinforcement from corrosion in reinforced ECC structures. Initial investigations into the use of hydrophobic agents in ECC were conducted by Martinola et al. [28].

Acknowledgement

Support by the NSF to the ACE-MRL and by the Deutsche Forschungsgemeinschaft (DFG) to M. Weimann to support his studies at the Univ. of Michigan are gratefully acknowledged.

References

1. Li, V. C.: *"Reflections on the Research and Development of Engineered Cementitious Composites"*, in: Proceedings of the JCI International Workshop on Ductile Fiber Reinforced Cementitious Composites (DFRCC) – Application and Evaluation, Japan Concrete Institute, pp. 1-22, (2002)
2. Crank, J.:*"The Mathematics of Diffusion"*, Oxford University Press, London, (1975)
3. Adamson, A. W.: *"Physical Chemistry of Surfaces"*, 6th Edition, John Wiley and Sons, Inc., (1997)
4. Wittmann, F. H.:*"Interaction of Hardened Cement Paste and Water"*, Journal of the American Ceramic Society, **56**, 8, pp. 409-415, (1973)
5. Weimann, M. B.: *"Vergleichende Studie der hygrischen Eigenschaften ausgewählter Werkstoffe des Bauwesens"*, Building Materials Reports No. 14, Aedificatio Verlag GmbH, Freiburg, Germany, (2001)
6. Brunauer, S., Emmett, P. H. and Teller E.: "Adsorption of Gases in Multimolecular Layers", Journal of American Chemical Society, pp. 309-319, (February 1938)

7. Beltzung, F., Wittmann, F. H. and Holzer L.: *"Influence of Composition of Pore Solution on Drying Shrinkage"*, in: Creep, Shrinkage and Durability Mechanics of Concrete and other Quasi-Brittle Materials, Eds. Ulm, F.-J., Bazant, Z .P. and Wittmann, F. H., Elsevier Science Ltd., pp. 39-48, (2001)
8. Derjaguin, B.V., Rabinovich, Y.I. and Churaev, N.V.: *"Direct Measurement of Molecular Forces"*, Nature, **272**, 5651, pp. 313-318, (1978)
9. Wittmann, F. H.: *"The Structure of Hardened Cement Paste - A Basis for a Better Understanding of the Materials Properties"*, in: Hydraulic Cement Paste: Their Structure and Properties, Cement and Concrete Association, Slough, United Kingdom, pp. 96-117, (1976)
10. Wittmann, F. H.: *"Creep and Shrinkage Mechanisms"*, in: Creep and Shrinkage in Concrete Structures, Eds. Z. Bazant and F. H. Wittmann, J. Wiley and Sons Inc., pp.129-161, (1982)
11. Schubert, H.: *"Kapillarität in porösen Feststoffsystemen"*, Springer-Verlag, Berlin, Germany, (1982)
12. Bangham, D. and Fakhoury, N.: *"The Translational Motion of Molecules in the Adsorbed Phase on Solids"*, Journal of the Chemical Society, Part I, pp. 1324-1333, (1931)
13. Hiller, K. H.: *"Strength Reduction and Length Changes in Porous Glass Caused by Water Vapour Adsorption"*, Journal of Applied Physics, **35**, 5, pp. 1622-1628, (1964)
14. Yates, D.J.C.: *"Molecular Specificity in Physical Adsorption"*, Advances in Catalysis and Related Subjects, **12**, pp. 265-312, Academic Press Inc., (1960)
15. Flood, E .A. and Heyding, R. D.: *"Stresses and Strains in Adsorbent-Adsorbate Systems"*, Canadian Journal of Chemistry, **32**, pp. 660-682, (1954)
16. Wittmann, F. H.: "*Surface Tension, Shrinkage and Strength of Hardened Cement Paste"*, Materials and Structures, **1**, 6, pp. 547-552, (1968)
17. Weimann, M. B. and Li, V. C.: *"Drying Shrinkage and Crack Width of an Engineered Cementitious Composite (ECC)"*, in: Brittle Matrix Composites 7, Woodhead Publishing Limited, Eds. A. M. Brandt, V. C. Li and I. H. Marshall, pp. 37-46, (2003)
18. Israelachvili, J. N.: *"Intermolecular and Surface Forces"*, Academic Press Inc., (1992)
19. Bazant, Z. P.: *"Mathematical Models for Creep and Shrinkage of Concrete",* in: Creep and Shrinkage in Concrete Structures, Eds. Bazant, Z. P. and Wittmann, F. H., Wiley, London, pp. 163-256, (1982)
20. Alvaredo, A. M.: *"Drying Shrinkage and Crack Formation"*, Building Materials Reports No. 4, Aedificatio Verlag GmbH, Freiburg, Germany, (1994)
21. Li, V. C., Wang, S. and Wu. C.: *"Tensile Strain-Hardening Behavior of Polyvinyl Alcohol Engineered Cementitious Composites (PVA-ECC)"*, **A**merican

Concrete **I**nstitute Materials Journal, pp. 483-492, (November-December 2001)

22. **A**merican **S**ociety for **T**esting and **M**aterials (U.S. Code Organization)
23. Greenspan, L.: *"Humidity Fixed Points of Binary Saturated Aqueous Solutions"*, Journal of Research of the National Bureau of Standard – American Physics Chemistry, **81A**, 1, (January-February 1977)
24. Schneider, A.: *"Diagramme zur Bestimmung der relativen Luftfeuchtigkeit"*, Holz als Roh- und Werkstoff (German Journal), **7**, pp. 269-272, (1960)
25. Shah, S. P., Karaguler, M.E. and Sarigaphuti, M.: *"Effect of Shrinkage-Reducing Admixtures on Restrained Shrinkage Cracking of Concrete"*, **A**merican **C**oncrete **I**nstitute Materials Journal, **89**, pp. 289-295, (May-June 1992)
26. Wittmann, F. H.: *"Structure and Fracture Mechanics of Composite Materials"*, in: Fracture Toughness and Fracture Energy, Eds. H. Mihashi, H. Takahashi and F. H. Wittmann, A.A. Balkema Publishers, pp. 3-12, (1989)
27. Wang, K., Jansen, D. C. and Shah, S. P.: *"Permeability Study of Cracked Concrete"*, Cement and Concrete Research, **27**, 3, pp. 381-393, (1997)
28. Martinola, G., Bäuml, M. and Wittmann F. H.: *"Modified ECC Applied as an Effective Chloride Barrier",* Proceedings of the JCI International Workshop on DFRCC, pp. 171-180, (2002)

Dr. M. B. Weimann studied physics at the University of Constance and at the Technical University of Berlin in Germany. He received a doctoral degree in Civil Engineering from the Swiss Federal Institute of Technology (ETH) in Zurich, Switzerland. Currently he is a scholar of the Deutsche Forschungsgemeinschaft (DFG) in the working group of Prof. Dr. V. C. Li at the University of Michigan in Ann Arbor, U.S.A. His research interest is the physical behavior and durability of building materials. weimann@engin.umich.edu

Prof. Dr. V. C. Li is a professor of Civil and Environmental Engineering at the University of Michigan, Ann Arbor, U.S.A. He is a fellow of the American Society of Civil Engineers and the American Society of Mechanical Engineers. His research interests include micromechanics, design, durability and mechanical performance of cement based composites, as well as environmental improvements through materials technology. vcli@engin.umich.edu

Received July 27th 2003